


Cryogenic Memory Element Based on an Anomalous Josephson Junction

C. Guarcello^{1,2,*} and F.S. Bergeret^{1,3}

¹*Centro de Física de Materiales, Centro Mixto CSIC-UPV/EHU, Paseo Manuel de Lardizabal 5, 20018 San Sebastián, Spain*

²*Dipartimento di Fisica “E.R. Caianiello”, Università di Salerno, Via Giovanni Paolo II, 132, I-84084 Fisciano, SA, Italy*

³*Donostia International Physics Center, Paseo Manuel de Lardizabal 4, 20018 San Sebastián, Spain*

 (Received 26 September 2019; revised manuscript received 16 January 2020; accepted 14 February 2020; published 4 March 2020)

We propose a nonvolatile memory element based on a lateral ferromagnetic Josephson junction with spin-orbit coupling and out-of-plane magnetization. The interplay between the latter and the intrinsic exchange field of the ferromagnet leads to a magnetoelectric effect that couples the charge current through the junction and its magnetization, such that by applying a current pulse the direction of the magnetic moment in F can be switched. The two memory states are encoded in the direction of the out-of-plane magnetization. With the aim to determine the optimal working temperature for the memory element, we explore the noise-induced effects on the averaged stationary magnetization by taking into account thermal fluctuations affecting both the Josephson phase and the magnetic moment dynamics. We investigate the switching process as a function of intrinsic parameters of the ferromagnet, such as the Gilbert damping and strength of the spin-orbit coupling, and propose a nondestructive readout scheme based on a dc superconducting quantum interference device. Additionally, we analyze a way to protect the memory state from external perturbations by voltage gating in systems with a both linear-in-momentum Rashba and Dresselhaus spin-orbit coupling.

DOI: [10.1103/PhysRevApplied.13.034012](https://doi.org/10.1103/PhysRevApplied.13.034012)

I. INTRODUCTION

Superconducting electronics is suggested as playing an important role in the search of ultra-low-power computers [1–5]. One of the key challenges towards this objective is the fabrication of a reliable and scalable cryogenic memory architecture. Superconductor-ferromagnet-superconductor (S - F - S) junctions are promising structures suggested for such memories [6–15]. Indeed, the interplay between the intrinsic exchange field and the induced superconductivity in the ferromagnet leads to the so-called π junction, i.e., a Josephson junction exhibiting an intrinsic π -phase shift in its ground state. Vertical ferromagnetic multilayer structures are being used as Josephson magnetic memories. The two logic states of these memories usually correspond to states with different relative orientation of magnetic layers, that in turn determines whether the junction is in the 0 or π state. Readout schemes are commonly based on distinguishing between resistive and nonresistive states.

Here, we delve into the alternative idea, initially suggested in Ref. [16], of designing a cryogenic memory element based on a ferromagnetic anomalous Josephson junction, usually called φ_0 junction [17]. It consists of a

S - F - S Josephson junction with a Rashba-like spin-orbit coupling (SOC). Its ground state corresponds to a finite phase shift in its current-phase-relation $0 < \varphi_0 < \pi$. Such an anomalous phase has been recently detected experimentally in hybrid Josephson junctions fabricated with the topological insulator Bi_2Se_3 [18] and Al/InAs heterostructures [19] and nanowires [20]. Both materials have strong spin-orbit coupling and in those experiments, time reversal is broken by an external magnetic field that acts as a Zeeman field. Here, the memory element is a Josephson junction with a ferromagnetic link, thus in principle time reversal is broken intrinsically by the exchange field. As demonstrated theoretically, in these junctions the magnetization of F can be controlled by passing an electric current through the device [16,21–26]. We discuss the use of such a junction as a memory element with the information encoded in the magnetization direction of the F layer. An important issue for the memory element is the effects stemming from the unavoidable thermal fluctuations on both phase and magnetization dynamics. Therefore, we present an exhaustive analysis of the noisy dynamics of a current-biased S - F - S Josephson junction, see Fig. 1, considering the influence of stochastic thermal fluctuations. Notably, in order to preserve gauge invariance the numerical model that we use to describe the phase dynamics includes also

*cguarcello@unisa.it

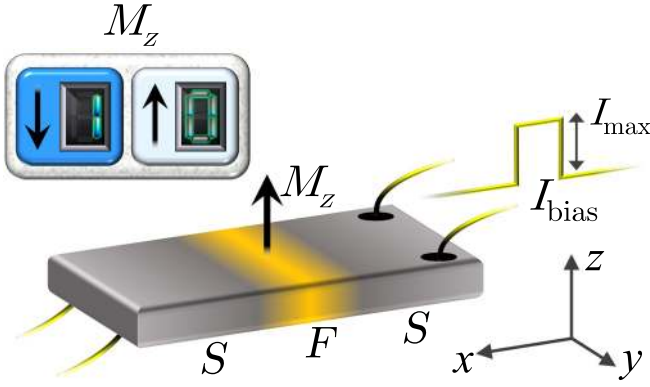


FIG. 1. S - F - S Josephson junction driven by a rectangular bias current pulses, I_{bias} , with amplitude I_{max} . The z component of the magnetization, M_z , is the observable used to define the logic memory states 0 and 1.

the time derivative of the anomalous phase, according to Ref. [27]. We explore the current-induced magnetic bistability, in order to define two well-distinguishable logic states, and investigate the robustness of such memory against noise-induced effects. We also suggest a suitable noninvasive readout scheme based on a current-controlled superconducting quantum interference device (SQUID), which does not require an additional magnetic flux to set the optimal operating point. Moreover, we discuss the intriguing possibility of effectively shielding the memory state by voltage gating, in a device formed by a ferromagnetic layer with a linear-in-momentum Dresselhaus spin-orbit coupling term.

The work is organized as follows: in Sec. II, we present the theoretical model used to describe the time evolution of both the magnetic moment and the Josephson phase of a current-driven S - F - S junction. In Sec. III we discuss the magnetic configuration of the junction after applying a current pulse. Specifically we determine its stationary magnetization, as a function of the Gilbert damping parameter and the SOC strength. In Sec. IV, we focus on the effect of stochastic thermal fluctuations on both the phase and the magnetization dynamics. In Sec. V, we explore how a generic Rashba-Dresselhaus-type SOC can affect the stationary magnetization. In Sec. VI, we discuss a feasible readout scheme based on a dc SQUID magnetometer. In Sec. VII we present our conclusions.

II. THE MODEL

We consider a similar setup as the one studied in Ref. [22]. It consists of a S - F - S junction in which the ferromagnet is a thin film with an out-of-plane magnetic anisotropy and a Rashba-like SOC, see Fig. 1.

Because of the interplay between the exchange field and the SOC, the current-phase relation of the S - F - S Josephson junction reads $I_\varphi = I_c \sin(\varphi - \varphi_0)$, where I_c is the critical

current of the junction, φ is the Josephson phase difference, and φ_0 is the so-called anomalous phase shift. The latter depends on several parameters of the system, such as the Rashba coefficient α [28,29], the transparency of S - F interfaces, the spin relaxation, and the disorder degree of the junction. The exact dependence on these parameters is not as crucial as the geometry of the device. If we consider a two-dimensional SOC with momenta in the plane of the F film, and the charge current flows in x direction, then the phase shift φ_0 is proportional to the y component of the magnetic moment according to Refs. [17,22,30,31]

$$\varphi_0 = r \frac{M_y}{M}, \quad (1)$$

where $M = \sqrt{M_x^2 + M_y^2 + M_z^2}$ is the modulus of the magnetization vector, and the parameter r quantifies the SOC strength and contains the α dependence. The specific dependence of r on the SOC is discussed in Sec. IV, when we consider the coexistence of both Rashba and Dresselhaus SOC contributions and their impact on the magnetization dynamics.

As discussed in Refs. [16,22,25,32], Eq. (1) establishes a direct coupling between the magnetic moment and the supercurrent. The time evolution of the magnetization can be described in terms of the Landau-Lifshitz-Gilbert (LLG) equation [33,34]

$$\frac{d\mathbf{M}}{d\tau} = -g_r \mathbf{M} \times \mathbf{H}_{\text{eff}} + \frac{\gamma}{M} \left(\mathbf{M} \times \frac{d\mathbf{M}}{d\tau} \right), \quad (2)$$

where g_r denotes the gyromagnetic ratio. The first term on the right-hand side describes the precession motion around \mathbf{H}_{eff} , whereas the second term describes the dissipation, which is accounted by the phenomenological dimensionless Gilbert damping parameter γ . The i th component of the effective field \mathbf{H}_{eff} , with $i = x, y, z$, can be calculated as [35]

$$H_{\text{eff},i} = -\frac{1}{\Omega} \frac{\partial \mathcal{F}}{\partial M_i}, \quad (3)$$

where Ω is the volume of the F layer, and \mathcal{F} is the free energy of the junction, which can be written as

$$\mathcal{F} = -E_J \varphi I_{\text{bias}} + E_s(\varphi, \varphi_0) + E_M. \quad (4)$$

Here, $E_J = \Phi_0 I_c / (2\pi)$ with Φ_0 being the flux quantum, I_{bias} is the external current in units of I_c , $E_s(\varphi, \varphi_0) = E_J [1 - \cos(\varphi - \varphi_0)]$, and $E_M = -\mathcal{K} \Omega / 2 (M_z / M)^2$ is the magnetic energy depending on the anisotropy constant \mathcal{K} . The ratio between the energy scales of the system is indicated by the parameter $\varepsilon = E_J / (\mathcal{K} \Omega)$.

The effective magnetic field calculated from Eq. (3) reads

$$\mathbf{H}_{\text{eff}} = \frac{\mathcal{K}}{M} [\varepsilon r \sin(\varphi - rm_y) \hat{y} + m_z \hat{z}], \quad (5)$$

with $m_{x,y,z} = M_{x,y,z}/M$.

Since the normalized components of the magnetization satisfy the condition $m_x^2 + m_y^2 + m_z^2 = 1$, it is convenient to write the LLG equations in spherical coordinates [36], so that the normalized components of the magnetization can be expressed in terms of the polar and azimuthal angles θ and ϕ as

$$\begin{aligned} m_x(\tau) &= \sin\theta(\tau) \cos\phi(\tau), \\ m_y(\tau) &= \sin\theta(\tau) \sin\phi(\tau), \\ m_z(\tau) &= \cos\theta(\tau). \end{aligned} \quad (6)$$

By normalizing the time to the inverse of the ferromagnetic resonance frequency $\omega_F = g_r \mathcal{K}/M$, that is $t = \omega_F \tau$, the LLG equations in spherical coordinates reduce to the following two coupled equations [36]

$$\frac{d\theta}{dt} = \frac{1}{1 + \gamma^2} (\tilde{H}_{\text{eff},\phi} + \gamma \tilde{H}_{\text{eff},\theta}), \quad (7)$$

$$\sin\theta \frac{d\phi}{dt} = \frac{1}{1 + \gamma^2} (\gamma \tilde{H}_{\text{eff},\phi} - \tilde{H}_{\text{eff},\theta}), \quad (8)$$

where the θ and ϕ components of the normalized effective field are defined as

$$\tilde{H}_{\text{eff},\theta} = \varepsilon r \sin(\varphi - rm_y) \cos\theta \sin\phi - m_z \sin\theta, \quad (9)$$

$$\tilde{H}_{\text{eff},\phi} = \varepsilon r \sin(\varphi - rm_y) \cos\phi. \quad (10)$$

Next, we discuss how the Josephson phase $\varphi(t)$ of a magnetic junction responds to a driving bias current. The dynamics of an overdamped S - F - S Josephson junction can be described through the modified resistively shunted junction (RSJ) model [27,37] generalized to include the anomalous phase shift $\varphi_0 = rm_y$. The phase dynamics is described by the following equation:

$$\frac{d\varphi}{dt} = \omega [I_{\text{bias}}(t) - \sin(\varphi - rm_y)] + r \frac{dm_y}{dt}, \quad (11)$$

where the time is still normalized to the inverse of the ferromagnetic resonance frequency and $\omega = \omega_J/\omega_F$, with $\omega_J = 2\pi I_c R/\Phi_0$ being the characteristic frequency of the junction [37] (R is the normal-state resistance of the device).

The last term in the right-hand side of Eq. (11) stems from the time derivative of the anomalous phase, $\dot{\varphi}_0$, cf. Eq. (1), and was ignored in Refs. [16], [22], and [25], but has to be included in order to preserve gauge invariance

[27]. The detailed derivation of this term can be found in the Supplemental Material of Ref. [27].

We assume that the S - F - S junction is driven by a rectangular current pulse, I_{bias} , centered at t_c :

$$I_{\text{bias}}(t) = \begin{cases} I_{\text{max}}, & t_c - \sigma \leq t \leq t_c + \sigma \\ 0, & \text{elsewhere.} \end{cases} \quad (12)$$

Here, σ is the width and I_{max} is the intensity, in units of I_c , of the pulse, so that a value $I_{\text{max}} > 1$ indicates a bias current larger than the critical value.

Because of the magnetoelectric effect in a φ_0 junction, the charge current induces an in-plane magnetic moment [30,31,38–41], which in turn acts as a torque on the out-of-plane magnetization of the F layer and eventually leads to its switching [16,22].

In the next sections we search for an optimal combination of system parameters to induce the magnetization reversal. Specifically, we explore the response of the magnetization by varying γ and r in suitable ranges, whereas the energy and timescales ratios ε and ω , are fixed. The energy ratio ε ranges from $\varepsilon \sim 100$ [22] in systems with weak magnetic anisotropy, to $\varepsilon \sim 1$ for stronger anisotropy [42]. In our calculation we choose an intermediate value $\varepsilon = 10$. The typical ferromagnet resonance frequency is $\omega_F \simeq 10$ GHz, while the characteristic Josephson frequency, usually of the order of gigahertz, may be tuned experimentally. Therefore, we choose $\omega = 1$. As long as the injected bias current is below the critical value, the results discussed in this work are only weakly affected by the value of ω . In contrast, if $I_{\text{bias}} > 1$ the magnetic switching would become more unlikely as ω increases. In particular, for $\omega \gg 1$ the torque exerted by the Josephson current oscillates very fast, in comparison with the timescale of the magnetization [23]. This means that the magnetization would experience an effective torque averaged over many oscillations, which results in a small contribution due to a partial cancellation of the net torque.

At $t = 0$ we assume that the F magnetization points towards the z direction, that is $\mathbf{M} = (0, 0, 1)$. With this initial values we solve Eqs. (7)–(8) and (11) self-consistently for different values of the parameters. From the solution we determine the magnetization direction after the current pulse.

III. THE DETERMINISTIC ANALYSIS

We first neglect the effect of thermal noise, as in Refs. [16] and [25], and explore the magnetic switching of the junction.

The overall behavior of the stationary magnetization m_z^{st} , namely, the value of m_z at the time $t = t_{\text{max}} = 100$, as a function of both the Gilbert damping parameter, γ , and the SOC strength, r , at different current pulse intensities I_{max} and $\sigma = 5$, is summarized in Fig. 2.

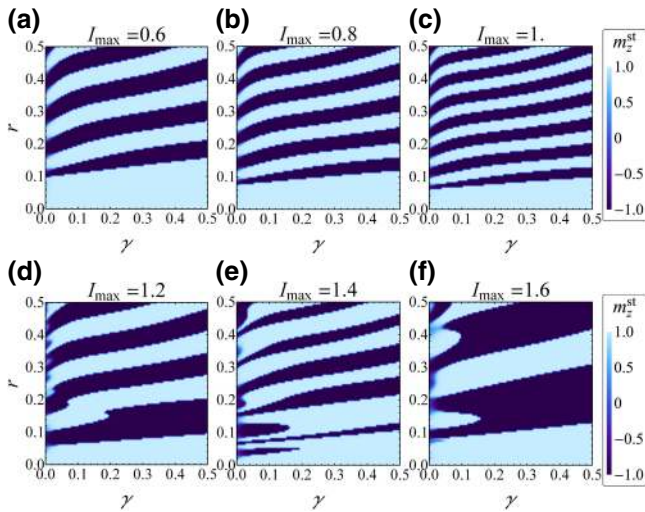


FIG. 2. Stationary magnetization, m_z^{st} , as a function of r and γ , at different values of the amplitude I_{max} of the current pulse, in the absence of noise fluctuations. The other parameters are $\varepsilon = 10$, $\omega = 1$, $\sigma = 5$, and $m_z(t = 0) = +1$.

We note that each contour plot is characterized by a dark-fringes pattern, namely, we observe regions of the (γ, r) parametric space in which the magnetization reversal systematically occurs, i.e., in which $m_z^{\text{st}} = -1$. This means, for instance, that by increasing r at a fixed γ we observe a sequence of $m_z^{\text{st}} = +1$ and $m_z^{\text{st}} = -1$ values.

For small enough r values, the magnetization reversal effect is absent. Interestingly, the pattern of dark fringes evidently changes for $I_{\text{max}} > 1$, so that for $I_{\text{max}} = 1.6$ the dark fringes merge together in large areas of (γ, r) values in which magnetization reversal takes place.

With the aim of selecting a driving pulse suitable for a memory application, we observe that the magnetization reversal effect should be sufficiently robust against small changes of both the current pulse intensity and the duration of the pulse. In Fig. 3 we show the stationary magnetization as a function of the pulse width σ , by changing the pulse amplitude I_{max} . We have chosen the parameters $r = 0.1$ and $\gamma = 0.25$. We observe that for a bias current below the critical value, the need for an accurate current-width regulation is significantly relaxed, since the magnetization reversal definitively occurs for any width above a specific value. Instead, for current amplitudes higher than the critical value, the stationary magnetization versus σ is highly scattered between the two possible values, $m_z^{\text{st}} = \pm 1$, so that even a slight change in the pulse width may lead to a nonswitching situation. To understand this behavior, we observe that, for a bias current higher than I_c , a pulse sufficiently long can make the junction to switch to the resistive state, so that the Josephson phase rapidly evolves and a voltage drop across the device appears, since $V \propto d\phi/dt$ [37]. In this case, the steady magnetization strongly depends on the dynamical state of the system when the

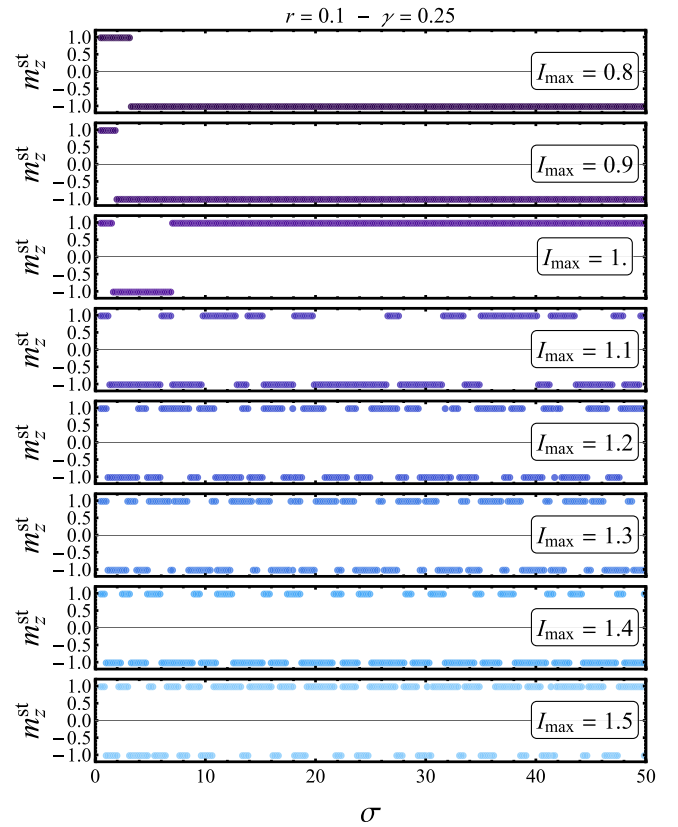


FIG. 3. Stationary magnetization, m_z^{st} , as a function of the current pulse width, σ , at different values of the amplitude $I_{\text{max}} \in [0.8-1.5]$, in the absence of noise fluctuations. The other parameters are $r = 0.1$, $\gamma = 0.25$, $\varepsilon = 10$, $\omega = 1$, and $m_z(t = 0) = +1$.

current pulse is switched off. Moreover, the higher the bias current is, the faster the Josephson phase evolves, and the more pronounced the σ dependence of m_z^{st} is. In view of a memory application, a current pulse smaller than the critical value is therefore recommended, in order to make the magnetization reversal unrelated on the pulse width σ . For these reasons in the subsequent analysis we set $I_{\text{max}} = 0.9$ and $\sigma = 5$ and focus on the thermal effect on the phase and the magnetization dynamics.

IV. EFFECTS OF NOISE

In this section, we focus on the noisy dynamics of the junction, specifically on how it affects the magnetization reversal. The temperature can significantly influence the time evolution of the system, eventually inducing unwanted magnetization flip or preventing a stable magnetization reversal. Therefore, we consider stochastic thermal fluctuations in both the phase and the magnetic moment dynamics. We start discussing the effect of a thermal noise source only on the phase within the RSJ model. In the second part of this section we include also the thermal noise on the magnetization dynamics.

A. Thermal-current effects on the RSJ model

The phase dynamics can be directly perturbed by thermal fluctuations accounted by adding to the RSJ model, Eq. (11), a Langevin Gaussianly distributed, delta-correlated stochastic term, $I_{\text{th}}(t)$. This “thermal current” has the usual white-noise statistical properties that, in normalized units, can be expressed as [37,43,44]

$$\langle I_{\text{th}}(t) \rangle = 0, \quad (13)$$

$$\langle I_{\text{th}}(t)I_{\text{th}}(t') \rangle = 2D_I \delta(t - t'). \quad (14)$$

Here, we introduce the dimensionless amplitude of thermal-current fluctuations defined as

$$D_I = \frac{k_B T \omega_F}{R I_c^2} = \frac{1}{\omega} \frac{k_B T}{E_J}. \quad (15)$$

For example, if $\omega = 1$ we obtain $D_I \sim 0.04(T/I_c)(\mu\text{A}/\text{K})$, so that, for instance, a junction with $I_c = 1 \mu\text{A}$ at $T = 250 \text{ mK}$ is affected by a thermal fluctuation of intensity $D_I \sim 10^{-2}$.

By taking into account the noise contribution, Eq. (11) becomes

$$\frac{d\varphi}{dt} = \omega [I_{\text{bias}}(t) - \sin(\varphi - r m_y) + I_{\text{th}}(t)] + r \frac{d m_y}{dt}. \quad (16)$$

In Fig. 4 we compare the current-induced magnetization reversal obtained without and with accounting of the noise effects, see (a) and (b), respectively. We set the intensity of the current pulse $I_{\text{max}} = 0.9$ and its width $\sigma = 5$.

In Fig. 4(a) we show the behavior of m_z^{st} as a function of r and γ in the deterministic case, namely, in the absence of noise, $D_I = 0$. Here, we observe a contour plot by many narrow dark fringes in which $m_z^{\text{st}} = -1$, see Fig. 4(a).

The situation drastically changes if we include the thermal noise. In this case we focus on the average stationary magnetization, $\overline{m_z^{\text{st}}}$, which is computed by averaging the stationary magnetization over $N_{\text{exp}} = 100$ independent numerical runs. The behavior of $\overline{m_z^{\text{st}}}$ as a function of r and γ for $D_I = 0.01$ is illustrated in Fig. 4(b). At small values of r the magnetization reversal is still absent, whereas noise mostly affects the regions with large r where the averaged value of the magnetization is mainly distributed around zero. Nevertheless, one can still identify dark regions in which magnetization switching takes place. With a red circle we highlight in Fig. 4(b) the region around the point $(\gamma, r) = (0.25, 0.1)$ where the magnetization takes the largest negative average magnetization $\overline{m_z^{\text{st}}} \simeq -1$. In other words, the region with the most robust switching.

By increasing the noise intensity the switching process is suppressed, as shown in Fig. 4(c), at the optimal values $r = 0.1$ and $\gamma = 0.25$ in Fig. 4(b). In Fig. 4(c) the value of $\overline{m_z^{\text{st}}}$ is the average over $N_{\text{exp}} = 1000$ independent numerical

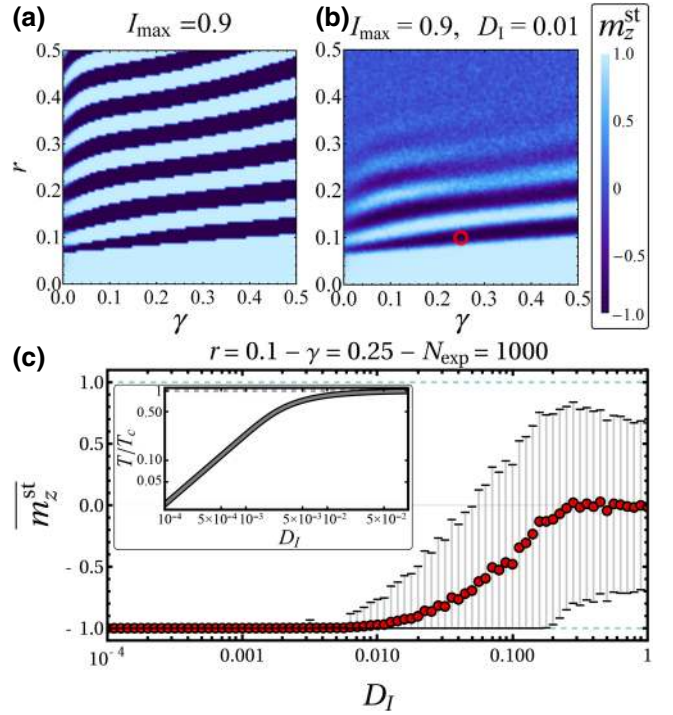


FIG. 4. (a) Stationary magnetization, m_z^{st} , as a function of r and γ . (b) Average stationary magnetization, $\overline{m_z^{\text{st}}}$, as a function of r and γ , at $D_I = 0.01$, calculated by averaging over $N_{\text{exp}} = 100$ independent numerical repetitions. (c) Average stationary magnetization, $\overline{m_z^{\text{st}}}$, as a function of the thermal-current intensity, D_I , at $\gamma = 0.25$ and $r = 0.1$ [namely, the (γ, r) values highlighted with a red circle in (b)], calculated by averaging over $N_{\text{exp}} = 1000$ independent numerical repetitions. The inset shows the normalized temperatures corresponding to the noise intensities D_I . For all panels $I_{\text{max}} = 0.9$ and $\sigma = 5$, whereas the values of other parameters are the same as those used to obtain Fig. 2.

repetitions. In the inset we show the normalized temperatures corresponding to the noise intensities D_I , calculated by assuming a junction with a temperature-dependent critical current and $I_c = 100 \mu\text{A}$ at low temperatures [45]. From this figure, one sees that $\overline{m_z^{\text{st}}} \simeq -1$ only for $D_I \lesssim 0.01$, that is for $T \lesssim 0.75T_c$. For higher noise intensities both the average magnetization and the error bar increase, approaching a zero magnetization average only for $D_I \gtrsim 0.3$.

In Fig. 5 we explore the time evolution of the different observables with and without thermal noise. Specifically, we show the response of the junction with $\gamma = 0.25$ and $r = 0.1$ to a current pulse with amplitude $I_{\text{max}} = 0.9$ depicted in (a). In the absence of noise, $D_I = 0$, we plot in Fig. 5(b) the time evolution of the phase and the supercurrent, and in Fig. 5(c) the different components of the magnetic moment. During the current pulse, i.e., the yellow shaded region, the phase first increases, and then it goes to zero when the pulse is turned off, see Fig. 5(b). To understand the phase behavior, we observe that, in the

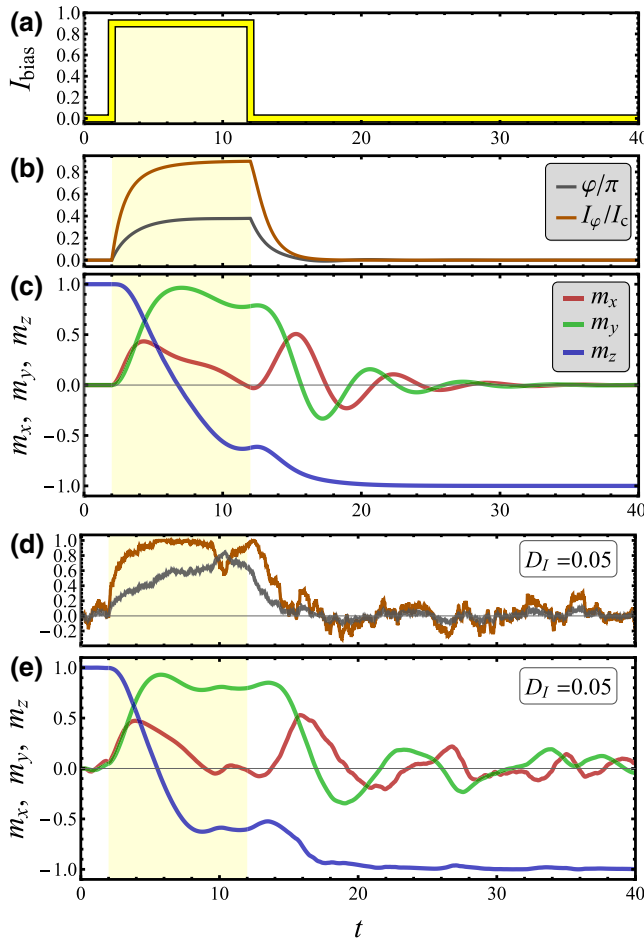


FIG. 5. Current pulse (a) and following time evolution of phase and Josephson current, see (b), and magnetization components, see (c), in the absence of noise and including a thermal-current contribution with amplitude $D_I = 0.05$, see (e),(d). The values of other parameters are $I_{\max} = 0.9$, $\sigma = 5$, $r = 0.1$, and $\gamma = 0.25$. The legends in (b),(c) refer also to (d),(e), respectively.

washboardlike picture [37], the tilting imposed by the bias current $I_{\max} = 0.9$ is not enough for allowing the “particle” to overcome the nearest potential barrier and switch the system to the finite voltage “running” state. Instead, the phase particle remains confined within a potential minimum, so that when the current is turned off, the slope of the washboard potential goes again to zero and the phase restores its initial position, i.e., $\varphi \rightarrow 0$.

We observe that the larger the bias current pulse, the higher the washboard potential slope, and therefore for $I_{\max} > 1$ the greater the speed of the phase particle, so that it can take a longer time to restore the initial position after the current pulse is switched off. Moreover, a large bias current pulse may also mean longer switching times. Hence, a current $I_{\max} < 1$ is, in general, more advantageous for a memory application.

In Fig. 5(c) we show how all components of the magnetization are induced by the current pulse. Whereas m_x

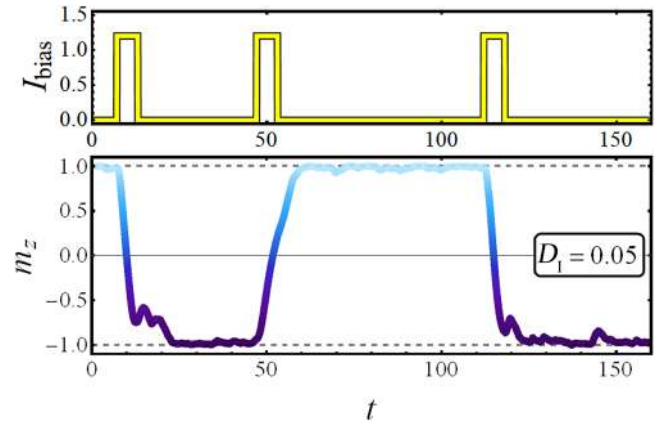


FIG. 6. Time evolution of the magnetization m_z , in response to a sequence of three current pulses shown in the top panel, in the presence of a thermal-current noise with amplitude $D_I = 0.05$. The values of the other parameters are $I_{\max} = 0.9$, $\sigma = 5$, $r = 0.1$, and $\gamma = 0.25$.

and m_y are generated during the current pulse, and they undergo a damped oscillations around zero when the current is switched off, the z component, after a transient regime, flips definitively to the value $m_z = -1$. From this figure we can also estimate the switching time $t_{\text{sw}} \simeq 10$, as the time m_z roughly takes to approach the value -1 after switching off the current.

The scenario described so far essentially persists also in the stochastic case, as shown in Figs. 5(d) and 5(e) for $D_I = 0.05$. Therefore, at the temperature that we are considering, the overall behavior is still quite similar to the one obtained in the absence of noise. In fact, the z component of the magnetization flips again to the value -1 , while the x and y components tend to oscillate around zero, without, however, vanishing definitively.

The magnetization switch can be achieved in a short time scale, by passing through the junction a sequence of current pulses, as it is shown in Fig. 6.

In the bottom panel we show the time evolution of the magnetization m_z , when the junction is excited by the three subsequent current pulses presented in the top panel, in the presence of a thermal-current noise with amplitude $D_I = 0.05$. In response to each current pulse, m_z follows first a transient regime, and then, as the current is switched off, it approaches the steady value with an opposite sign.

B. Effect of thermal noise on the magnetization dynamics

Thermal noise also affects directly the magnetization dynamics [46–51] via a stochastic field H_{th} , a sort of “thermal field,” which is added to the effective magnetic field term in Eq. (2), as done in Ref. [52]. Inclusion of the

thermal noise in Eq. (2) leads to [36]

$$\frac{d\mathbf{M}}{d\tau} = -g_r \mathbf{M} \times (\mathbf{H}_{\text{eff}} + \mathbf{H}_{\text{th}}) + \frac{\gamma}{M} \left(\mathbf{M} \times \frac{d\mathbf{M}}{d\tau} \right). \quad (17)$$

This stochastic differential equation has to be solved numerically by a stochastic integration prescription by keeping the modulus of the magnetic moment constant during the time evolution (see Ref. [36] and references therein). For this purpose it is again convenient to write the equations in spherical coordinates, see Eq. (6), so that the stochastic LLG equation reads [36,53]

$$\frac{d\theta}{dt} = \frac{1}{1 + \gamma^2} \left[\tilde{H}_{\text{eff},\phi} + \tilde{H}_{\text{th},\phi} + \gamma (\tilde{H}_{\text{eff},\theta} + \tilde{H}_{\text{th},\theta}) \right], \quad (18)$$

$$\sin \theta \frac{d\phi}{dt} = \frac{1}{1 + \gamma^2} \left[\gamma (\tilde{H}_{\text{eff},\phi} + \tilde{H}_{\text{th},\phi}) - \tilde{H}_{\text{eff},\theta} - \tilde{H}_{\text{th},\theta} \right], \quad (19)$$

where

$$\tilde{H}_{\text{th},\theta} = \tilde{H}_{\text{th},x} \cos \theta \cos \phi + \tilde{H}_{\text{th},y} \cos \theta \sin \phi - \tilde{H}_{\text{th},z} \sin \theta, \quad (20)$$

$$\tilde{H}_{\text{th},\phi} = -\tilde{H}_{\text{th},x} \sin \phi + \tilde{H}_{\text{th},y} \cos \phi. \quad (21)$$

The normalized field, $\tilde{\mathbf{H}}_{\text{th}} = (M/\mathcal{H})\mathbf{H}_{\text{th}}$ is assumed to be a Gaussianly distributed random field with the following statistical features

$$\langle \tilde{H}_{\text{th},i}(t) \rangle = 0 \quad (22)$$

$$\langle \tilde{H}_{\text{th},i}(t) \tilde{H}_{\text{th},i}(t') \rangle = 2D_H \delta(t - t'), \quad (23)$$

where $i = x, y, z$ and

$$D_H = \left(\frac{\gamma}{M} \frac{k_B T}{|g_r| \Omega} \right) \left(\frac{M}{\mathcal{H}} \right)^2 \omega_F = \gamma \frac{k_B T}{\mathcal{H} \Omega} \quad (24)$$

is the dimensionless amplitude of thermal-field fluctuations. In all previous equations the time is still normalized to the inverse of ω_F .

Interestingly, by recalling the definition of the parameter $\varepsilon = E_J/(\mathcal{H} \Omega)$, from Eqs. (15) and (24) we can easily obtain the following relation between the normalized thermal noise intensities

$$D_H = (\gamma \varepsilon \omega) D_I. \quad (25)$$

Thus, by changing the magnetization energy, the Gilbert damping parameter, or the magnetic resonance frequency we can effectively modify the relative strength of the two noise mechanisms. This means that one could optimize the system parameters in such a way to make, for instance, the

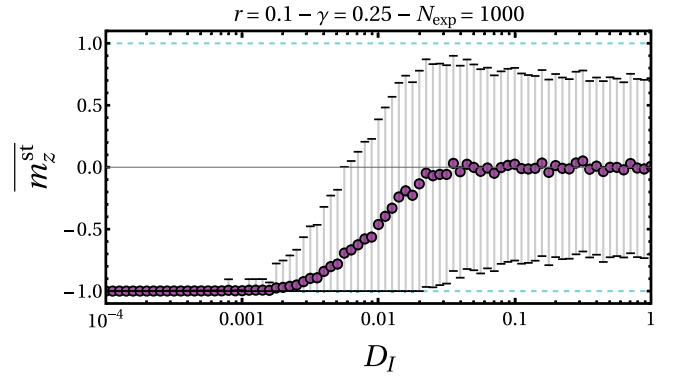


FIG. 7. Average stationary magnetization, $\overline{m_z^{\text{st}}}$, as a function of the noise intensity, D_I , calculated by taking into account both the thermal-current and the thermal-field noise contribution, and by averaging over $N_{\text{exp}} = 1000$ independent numerical repetitions. The values of other parameters are $I_{\text{max}} = 0.9$, $\sigma = 5$, $r = 0.1$, and $\gamma = 0.25$.

impact of the thermal field negligible with respect to the thermal current. This allows us to study the effects produced by these noise sources independently. In the following, even if we explicitly write only the value of D_I , we are taking into account both thermal-current and thermal-field-independent noise sources, whose amplitudes are related by Eq. (25).

The overall effect of both the thermal current and field is presented in Fig. 7, where we show the behavior of $\overline{m_z^{\text{st}}}$, calculated by averaging over $N_{\text{exp}} = 1000$ independent numerical runs, at different values of the noise intensity D_I , and by setting $I_{\text{max}} = 0.9$, $\sigma = 5$, $\gamma = 0.25$, and $r = 0.1$. We observe that the average magnetization remains close to the value $\overline{m_z^{\text{st}}} \simeq -1$ only for $D_I \lesssim 0.003$, that is for $T \lesssim 0.58T_c$, see the inset of Fig. 4(c). For larger values of D_I , $\overline{m_z^{\text{st}}}$ approaches zero and hence the magnetization reversal probability is reduced, Fig. 4(c). In view of the memory application, one should, in principle, carefully choose the F layer and its characteristics (such as its volume or the Gilbert damping parameter) in order to make the thermal-field effect as small as possible. The aim is to reduce the thermal-field intensity in order to increase the working temperature suitable for a memory application, e.g., through a lower Gilbert damping or a larger F volume, according to Eq. (25).

The time evolution of φ , I_φ , and m_i (with $i = x, y, z$), as the junction dynamics if affected by both a thermal current and a thermal field, for $r = 0.1$, $\gamma = 0.25$, and $D_I = 0.005$, is shown in Fig. 8.

Here, we consider again the system excited by a current pulse with intensity $I_{\text{max}} = 0.9$, as that one shown in Fig. 5(a). We observe that all noisy curves still resemble, in shape, the deterministic evolution presented in Figs. 5(b) and 5(c). The value $t_{\text{sw}} \simeq 10$ is a quite good estimation for the switching time of the device also in this noisy case.

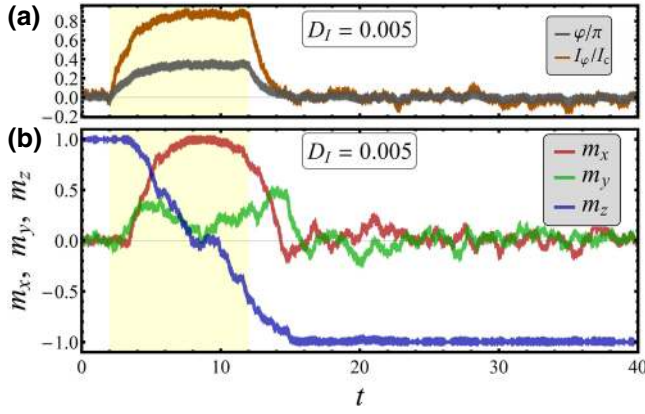


FIG. 8. Time evolution of phase and Josephson current (a) and magnetization components (b) as the system is excited by the current pulse in Fig. 5. Here we are taking into account both a thermal-current and a thermal-field contribution, with noise intensity $D_I = 0.005$. The values of other parameters are $I_{\max} = 0.9$, $\sigma = 5$, $r = 0.1$, and $\gamma = 0.25$.

V. RASHBA-DRESSELHAUS SOC

In all previous analysis it was assumed a pure Rashba SOC. However, the theory of φ_0 junctions can be generalized for any linear-in-momentum SOC [30,31], by using the SU(2)-covariant formulation [31], where the SOC is described in terms of a SU(2) vector potential \mathcal{A} . For a 2D SOC with both Rashba and Dresselhaus contributions one obtains $\mathcal{A}_x = -\alpha\sigma^y + \beta\sigma^x$ and $\mathcal{A}_y = \alpha\sigma^x - \beta\sigma^y$ (here, α and β are the Rashba and Dresselhaus coefficients and σ^x and σ^y are the first two Pauli matrices).

The appearance of the anomalous phase is related to the existence of a finite Lifshitz invariant term in the free energy [17,54–56], which is proportional to $T_i\partial_i\varphi$, where T_i is the i th component of a polar vector, which is odd under time reversal, ∂_i is the i th derivative of the superconducting phase, and the sum over repeated indices is implied here and below. For the particular junction geometry sketched in Fig. 1 the supercurrent, and hence the phase gradient, is finite in x direction. Thus, according to Eq. (5.17) of Ref. [30], the anomalous phase can be written in the following compact form [30,31]:

$$\varphi_0 = r_{\tilde{\beta}}(\tilde{\beta}m_x + m_y). \quad (26)$$

Here, we define the SOC coefficients' ratio, $\tilde{\beta} = \beta/\alpha$, and the parameter $r_{\tilde{\beta}} = r(1 - \tilde{\beta}^2)$, with r depending this time on both α and β . In the absence of the Dresselhaus SOC, that is when $\tilde{\beta} = 0$ and $r_{\tilde{\beta}} \rightarrow r$, we recover Eq. (1). If both contributions are similar in magnitude, i.e., when $\tilde{\beta} \rightarrow 1$, since $r_{\tilde{\beta}} \rightarrow 0$ the phase shift vanishes, i.e., $\varphi_0 \rightarrow 0$. This is a very interesting situation that we explore in this section. In fact, whereas the Dresselhaus contribution is due to the breaking of crystal inversion symmetries, the Rashba SOC stems from structural broken symmetry and therefore can

be controlled by a gate voltage [57,58]. In other words, a voltage gate can control the ratio $\tilde{\beta}$ between Dresselhaus and Rashba coefficients, and hence the phase shift and the supercurrent flow, according to Eq. (26). Specifically, by tuning α such that $\tilde{\beta} \simeq 1$ one can fully decouple the phase and magnetic moment dynamics. Such a process can be eventually used to protect the memory state in one of the storage elements of a distributed architecture.

We provide next a quantitative analysis of this situation, so that by taking into account the generic φ_0 , Eq. (26), into the expression for the effective field, Eq. (5) becomes

$$\mathbf{H}_{\text{eff}} = \frac{\mathcal{K}}{M} \{ \varepsilon r_{\tilde{\beta}} \sin[\varphi - r_{\tilde{\beta}}(\tilde{\beta}m_x + m_y)] (\tilde{\beta}\hat{x} + \hat{y}) + m_z\hat{z} \}. \quad (27)$$

The θ and ϕ components of the normalized effective field to be included in LLG Eqs. (7)–(8), read

$$\begin{aligned} \tilde{H}_{\text{eff},\theta} &= \varepsilon r_{\tilde{\beta}} \cos\theta \sin[\varphi - r_{\tilde{\beta}}(\tilde{\beta}m_x + m_y)] (\tilde{\beta}\cos\phi + \sin\phi) \\ &\quad - m_z \sin\theta, \end{aligned} \quad (28)$$

$$\tilde{H}_{\text{eff},\phi} = \varepsilon r_{\tilde{\beta}} \sin[\varphi - r_{\tilde{\beta}}(\tilde{\beta}m_x + m_y)] (\cos\phi - \tilde{\beta}\sin\phi), \quad (29)$$

whereas the RSJ equation becomes

$$\begin{aligned} \frac{d\varphi}{dt} &= \omega \{ I_{\text{bias}}(t) - \sin[\varphi - r_{\tilde{\beta}}(\tilde{\beta}m_x + m_y)] \} \\ &\quad + r_{\tilde{\beta}} \left(\tilde{\beta} \frac{dm_x}{dt} + \frac{dm_y}{dt} \right). \end{aligned} \quad (30)$$

The behavior of the stationary magnetization as a function of r and γ , at different values of $\tilde{\beta} \in [0 - 1]$ is shown in Fig. 9. The current pulse intensity and width are chosen equal to $I_{\max} = 0.9$ and $\sigma = 5$, respectively. As expected from the discussion above, the region where no magnetization switching occurs, bright color in Fig. 9, increases by increasing $\tilde{\beta}$ towards 1. For $\tilde{\beta} = 1$, the φ_0 behavior is fully suppressed, cf. Eq. (26), and hence no magnetization switching takes place, despite the current pulse flowing through the junction. Interestingly, we note that for intermediate values of $\tilde{\beta}$, the area of the switching fringes, i.e., where $m_z^{\text{st}} = -1$, increases considerably.

In summary of this section, by tuning $\alpha = \beta$ one can decouple the magnetic behavior from the Josephson dynamics and freeze the memory state in order to protect it from external current pulses and other perturbations. The major challenge in this regard is to find materials with a sizable magnetic moment and tunable by means of a gate voltage.

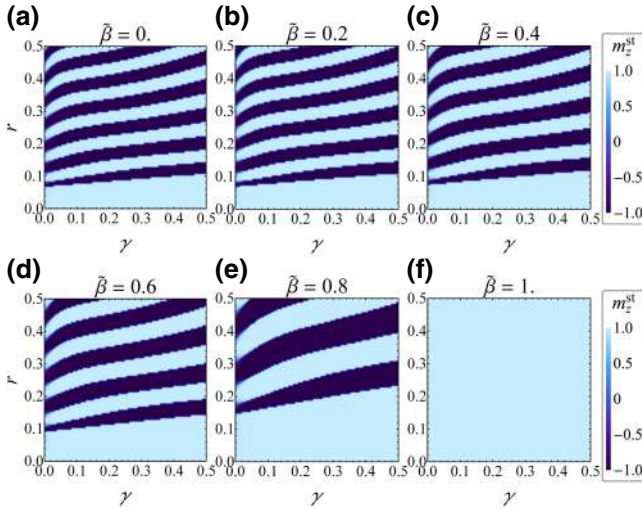


FIG. 9. Stationary magnetization, m_z^{st} , as a function of r and γ , at different values of the relative Dresselhaus coefficient $\tilde{\beta} = \beta/\alpha$, in the absence of noise fluctuations, by imposing $I_{\text{max}} = 0.9$ and $\sigma = 5$.

VI. THE MEMORY READOUT

As discussed in the previous section, the writing operation of the proposed memory element can be performed by exciting the junction with controlled current pulses. We could envisage an array of φ_0 -junction-based memory elements, each one eventually having its own current line so that it can be written by sending individual current inputs. Alternatively, exploiting the tuning of the SOC discussed in the previous section, one could control locally, via individual gates at each junction, several memory elements connected in series to a common current line. In this way one could selectively write via a common current pulse only a specific set of memory units.

The readout of the memory state can be nondestructively performed by direct measurement of the magnetization state through a dc SQUID inductively coupled to the φ_0 junction. A SQUID is essentially a magnetic flux detector [59], which can be employed to measure with a very high sensitivity any physical quantity that can be converted in a magnetic flux [60].

We suggest a SQUID sensor along the lines of the readout scheme implemented in Ref. [13] for a π -junction memory. Our scheme is based on an asymmetric inductive dc SQUID, which consists of a superconducting ring with a non-negligible total inductance, L , with two Josephson junctions with different critical currents, i.e., $I_{c,1} \neq I_{c,2}$ (here, we are neglecting for simplicity any asymmetry in the ring inductance). With such an asymmetric SQUID, one can avoid the use of an additional magnetic flux to adjust the working point of the device in a high-sensitivity position of the $I_c^{\text{SQUID}} - \Phi$ characteristics, where I_c^{SQUID} is the SQUID critical current and Φ is the magnetic flux threading the loop. In fact, such an asymmetric dc SQUID

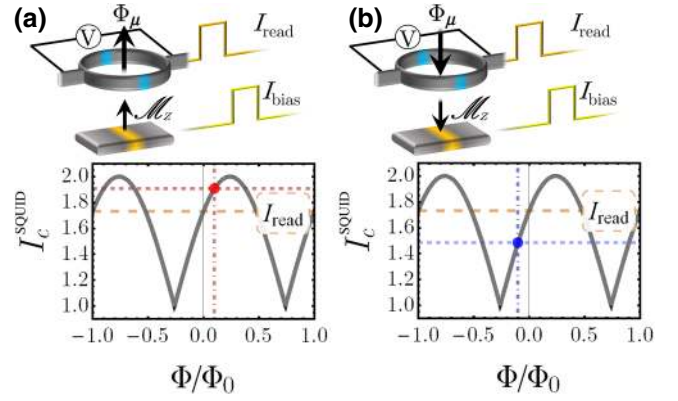


FIG. 10. SQUID-based memory readout and cartoon showing the critical current interference pattern of the SQUID, in the cases of both positive and negative orientation along the z axis of the magnetic moment, see (a),(b), respectively.

shows non-negligible screening and asymmetry parameters, that is $\beta_L = (2\pi/\Phi_0)(L/2)(I_{c,1} + I_{c,2}) \neq 0$ and $\alpha_I = (I_{c,1} - I_{c,2})/(I_{c,1} + I_{c,2}) \neq 0$, respectively. In this case, the I_c^{SQUID} maximum is not centered in $\Phi = 0$, but shifted from zero by $\Delta\Phi$, see Fig. 10, where [59] $2\pi\Delta\Phi = \Phi_0\beta_L\alpha_I$. Accordingly, our readout SQUID demonstrates a high-sensitivity point of the $I_c^{\text{SQUID}} - \Phi$ characteristics also in $\Phi = 0$, that is in the absence of an external magnetic flux.

We assume that the unbiased critical current, $I_c^0 = I_c^{\text{SQUID}}(\Phi = 0)$, lies in the positive branch of the critical current diffraction pattern of the SQUID, that is $dI_c^{\text{SQUID}}/d\Phi|_{\Phi=0} > 0$, just like in the case shown in Fig. 10. Thus, the magnetic moment $m_z = +1$ generates a positive magnetic flux $\Phi = +\Phi_\mu$ through the loop, and gives a critical current higher than the unbiased value, i.e., $I_c^+ = I_c^{\text{SQUID}}(+\Phi_\mu) > I_c^0$, see the red dashed line in Fig. 10(a). Conversely, if $m_z = -1$ the magnetic flux through the loop is negative, i.e., $\Phi = -\Phi_\mu$, and the critical current is lower than the unbiased value, $I_c^- = I_c^{\text{SQUID}}(-\Phi_\mu) < I_c^0$, see the blue dashed line in Fig. 10(b).

The SQUID readout loop is then sensed by passing a bit-read current with intensity $I_{\text{read}} = I_c^0$ through the device, see the orange dashed line in Fig. 10, that is a current, which lays in between I_c^- and I_c^+ . In this way, if the magnetic moment points in the negative z direction, which encodes the “1” logic state of the memory, the bit-read current makes the SQUID switch to the voltage state, since $I_{\text{read}} > I_c^-$. Consequently, a voltage drop appears across the readout SQUID in response to the bit-read current. For the opposite magnetic moment orientation, which encodes the “0” logic state, the SQUID critical current is larger than the bit-read current, that is $I_{\text{read}} < I_c^+$, so that the SQUID remains in the superconducting, zero-voltage state.

To provide an estimate of the dimensions of a SQUID loop suitable to detect the magnetic moment reversal we

consider the simple case of a circular readout SQUID with radius a and a magnetic moment oriented along the z axis and placed on the symmetry axis of the SQUID at a height z' above the x - y plane. In this case, the total magnetic flux through the loop can be estimated as [60,61] $\Phi_\mu = (\mu_0 M_z / 2) a^2 / (a^2 + z'^2)^{3/2}$. This flux is maximum at $z' = 0$ where it reads $\Phi_\mu = \mu_0 M_z / d$, with $d = 2a$ being the loop diameter. If we assume a saturation magnetization [62] $M = 8 \times 10^5$ A/m and a volume $\Omega = (10 \times 100 \times 100) \text{ nm}^3 = 10^{-22} \text{ m}^3$, we get a total magnetic moment $\mathcal{M}_z = 8 \times 10^{-17} \text{ A m}^2$ (that is $\mathcal{M}_z = 8.6 \times 10^6 \mu_B$, with μ_B being the Bohr magneton), so that the total magnetic flux reads $\Phi_\mu = 32\pi 10^{-24} d^{-1} \text{ Wb m}$. Thus, for a SQUID with diameter $\simeq 0.5 \mu\text{m}$ we obtain a measurable flux $\Phi_\mu \simeq \Phi_0 / 10$, (see vertical dot-dashed lines in Fig. 10).

VII. CONCLUSIONS

In conclusion, we discuss a nonvolatile superconducting memory based on a bistable magnetic behavior of a current-biased φ_0 junction, that is a superconductor-ferromagnet-superconductor Josephson junction with a Rashba-like spin-orbit coupling. The memory state is encoded in the magnetization direction of the ferromagnetic layer, which can be switched via controlled current pulses. Following Ref. [27], the numerical approach that we use to describe the phase dynamics of a current-driven ferromagnetic Josephson junction is amended to include the time derivative of the anomalous phase. We explore the robustness of the current-induced magnetization reversal against thermal fluctuations, in order to find the optimal working temperature at which the magnetization switching induced by a current pulse is stable. We also suggest a way of decoupling the Josephson phase and the magnetization dynamics, by tuning the Rashba SOC strength via a gate voltage.

Finally, we discuss a suitable nondestructive readout scheme based on a dc SQUID inductively coupled to the φ_0 junction. The suggested readout scheme is exclusively controlled by current pulses, and no additional magnetic flux is needed.

ACKNOWLEDGMENTS

This work is supported by the Horizon Research and Innovation Program under Grant Agreement No. 800923 (SUPERTED) and the Spanish Ministerio de Economía, Industria y Competitividad (MINEICO) under Project No. FIS2017-82804-P.

[1] Q. P. Herr, A. Y. Herr, O. T. Oberg, and A. G. Ioannidis, Ultra-low-power superconductor logic, *J. Appl. Phys.* **109**, 103903 (2011).

- [2] S. Nishijima, S. Eckroad, A. Marian, K. Choi, W. S. Kim, M. Terai, Z. Deng, J. Zheng, J. Wang, K. Umemoto *et al.*, Superconductivity and the environment: A roadmap, *Supercond. Sci. Technol.* **26**, 113001 (2013).
- [3] K. K. Likharev and V. K. Semenov, RSFQ logic/memory family: A new Josephson-junction technology for sub-terahertz-clock-frequency digital systems, *IEEE Trans. Appl. Supercond.* **1**, 3 (1991).
- [4] O. A. Mukhanov, Energy-efficient single flux quantum technology, *IEEE Trans. Appl. Supercond.* **21**, 760 (2011).
- [5] D. S. Holmes, A. L. Ripple, and M. A. Manheimer, Energy-efficient superconducting computing—power budgets and requirements, *IEEE Trans. Appl. Supercond.* **23**, 1701610 (2013).
- [6] A. K. Feofanov, V. A. Oboznov, V. V. Bol'ginov, J. Lisenfeld, S. Poletto, V. V. Ryazanov, A. N. Rossolenko, M. Khapipov, D. Balashov, A. B. Zorin, P. N. Dmitriev, V. P. Koshelets, and A. V. Ustinov, Implementation of superconductor/ferromagnet/superconductor π -shifters in superconducting digital and quantum circuits, *Nat. Phys.* **6**, 593 (2010).
- [7] V. V. Ryazanov, V. V. Bol'ginov, D. S. Sobanin, I. V. Vernik, S. K. Tolpygo, A. M. Kadin, and O. A. Mukhanov, Magnetic Josephson junction technology for digital and memory applications, *Phys. Procedia* **36**, 35 (2012).
- [8] T. E. Golikova, F. Hübler, D. Beckmann, I. E. Batov, T. Yu. Karminskaya, M. Yu. Kupriyanov, A. A. Golubov, and V. V. Ryazanov, Double proximity effect in hybrid planar superconductor-(normal metal/ferromagnet)-superconductor structures, *Phys. Rev. B* **86**, 064416 (2012).
- [9] B. Baek, William H. Rippard, S. P. Benz, S. E. Russek, and P. D. Dresselhaus, Hybrid superconducting-magnetic memory device using competing order parameters, *Nat. Commun.* **5**, 3888 (2014).
- [10] T. Golod, A. Iovan, and V. M. Krasnov, Single Abrikosov vortices as quantized information bits, *Nat. Commun.* **6**, 8628 (2015).
- [11] E. C. Gingrich, B. M. Niedzielski, J. A. Glick, Y. Wang, D. L. Miller, R. Loloee, W. P. Pratt, Jr., and N. O. Birge, Controllable 0 - π Josephson junctions containing a ferromagnetic spin valve, *Nat. Phys.* **12**, 564 (2016).
- [12] Bethany M. Niedzielski, T. J. Bertus, Joseph A. Glick, R. Loloee, W. P. Pratt, and Norman O. Birge, Spin-valve Josephson junctions for cryogenic memory, *Phys. Rev. B* **97**, 024517 (2018).
- [13] I. M. Dayton, T. Sage, E. C. Gingrich, M. G. Loving, T. F. Ambrose, N. P. Siwak, S. Keebaugh, C. Kirby, D. L. Miller, A. Y. Herr, Q. P. Herr, and O. Naaman, Experimental demonstration of a Josephson magnetic memory cell with a programmable π -junction, *IEEE Magn. Lett.* **9**, 1 (2018).
- [14] G. De Simoni, E. Strambini, J. S. Moodera, F. S. Bergeret, and F. Giazotto, Toward the absolute spin-valve effect in superconducting tunnel junctions, *Nano Lett.* **18**, 6369 (2018).
- [15] R. de Andrés Prada, T. Golod, O. M. Kapran, E. A. Borodianskyi, Ch. Bernhard, and V. M. Krasnov, Memory-functionality superconductor/ferromagnet/superconductor junctions based on the high- T_c cuprate superconductors $\text{YBa}_2\text{Cu}_3\text{O}_{7-x}$ and the colossal magnetoresistive manganite

- ferromagnets $\text{La}_2/3\text{X}_1/3\text{MnO}_{3+\delta}$ ($X = \text{Ca}, \text{Sr}$), *Phys. Rev. B* **99**, 214510 (2019).
- [16] Yu. M. Shukrinov, I. R. Rahmonov, K. Sengupta, and A. Buzdin, Magnetization reversal by superconducting current in φ_0 Josephson junctions, *Appl. Phys. Lett.* **110**, 182407 (2017).
- [17] A. Buzdin, Direct Coupling Between Magnetism and Superconducting Current in the Josephson φ_0 Junction, *Phys. Rev. Lett.* **101**, 107005 (2008).
- [18] A. Assouline, C. Feuillet-Palma, N. Bergeal, T. Zhang, A. Mottaghizadeh, A. Zimmers, E. Lhuillier, M. Eddrie, P. Atkinson, M. Aprili *et al.*, Spin-orbit induced phase-shift in Bi_2Se_3 Josephson junctions, *Nat. Commun.* **10**, 126 (2019).
- [19] W. Mayer, M. C. Dartailh, J. Yuan, K. S. Wickramasinghe, E. Rossi, and J. Shabani, Gate controlled anomalous phase shift in Al/InAs Josephson junctions, *Nat. Commun.* **11**, 212 (2020).
- [20] E. Strambini, A. Iorio, O. Durante, R. Citro, C. Sanz-Fernández, C. Guarcello, I. V. Tokatly, A. Braggio, M. Rocci, N. Ligato, V. Zannier, L. Sorba, F. S. Bergeret, and F. Giazotto, A Josephson quantum phase battery, *arXiv:2001.03393* (2020).
- [21] X. Waintal and P. W. Brouwer, Magnetic exchange interaction induced by a Josephson current, *Phys. Rev. B* **65**, 054407 (2002).
- [22] F. Korschelle and A. Buzdin, Magnetic Moment Manipulation by a Josephson Current, *Phys. Rev. Lett.* **102**, 017001 (2009).
- [23] J. Linder and T. Yokoyama, Supercurrent-induced magnetization dynamics in a Josephson junction with two misaligned ferromagnetic layers, *Phys. Rev. B* **83**, 012501 (2011).
- [24] I. V. Bobkova, A. M. Bobkov, and M. A. Silaev, Spin torques and magnetic texture dynamics driven by the supercurrent in superconductor/ferromagnet structures, *Phys. Rev. B* **98**, 014521 (2018).
- [25] Y. M. Shukrinov, I. R. Rahmonov, and A. E. Botha, Superconducting spintronics in the presence of spin-orbital coupling, *IEEE Trans. Appl. Supercond.* **28**, 1 (2018).
- [26] A. A. Mazanik, I. R. Rahmonov, and Y. M. Shukrinov, Analytical criteria for magnetization reversal in φ_0 Josephson junction, *arXiv:1910.04419* (2019).
- [27] D. S. Rabinovich, I. V. Bobkova, A. M. Bobkov, and M. A. Silaev, Resistive State of Superconductor-Ferromagnet-Superconductor Josephson Junctions in the Presence of Moving Domain Walls, *Phys. Rev. Lett.* **123**, 207001 (2019).
- [28] E. I. Rashba, Properties of semiconductors with an extremum loop. I. Cyclotron and combinational resonance in a magnetic field perpendicular to the plane of the loop, *Sov. Phys. Solid State* **2**, 1109 (1960).
- [29] Y. A. Bychkov and É. I. Rashba, Properties of a 2d electron gas with lifted spectral degeneracy, *JETP Lett.* **39**, 78 (1984).
- [30] F. Korschelle, I. V. Tokatly, and F. S. Bergeret, Theory of the spin-galvanic effect and the anomalous phase shift φ_0 in superconductors and Josephson junctions with intrinsic spin-orbit coupling, *Phys. Rev. B* **92**, 125443 (2015).
- [31] F. S. Bergeret and I. V. Tokatly, Theory of diffusive φ_0 Josephson junctions in the presence of spin-orbit coupling, *EPL (Europhys. Lett.)* **110**, 57005 (2015).
- [32] P. K. Atanasova, S. A. Panayotova, I. R. Rahmonov, Y. M. Shukrinov, E. V. Zemlyanaya, and M. V. Bashashin, Periodicity in the appearance of intervals of the reversal of the magnetic moment of a φ_0 Josephson junction, *Jetp Lett.* **110**, 722 (2019).
- [33] L. D. Landau and E. M. Lifshitz, On the theory of magnetic permeability dispersion in ferromagnetic solids, *Phys. Z. Sowjetunion* **8**, 153 (1935).
- [34] T. L. Gilbert, A phenomenological theory of damping in ferromagnetic materials, *IEEE Trans. Magn.* **40**, 3443 (2004).
- [35] E. M. Lifshitz and L. P. Pitaevskii, *Course of Theoretical Physics, Theory of the Condensed State* (Butterworth Heinemann, Oxford, 1990), Vol. 9.
- [36] F. Romá, L. F. Cugliandolo, and G. S. Lozano, Numerical integration of the stochastic Landau-Lifshitz-Gilbert equation in generic time-discretization schemes, *Phys. Rev. E* **90**, 023203 (2014).
- [37] A. Barone and G. Paternò, *Physics and Applications of the Josephson Effect* (Wiley, New York, 1982).
- [38] V. M. Edelstein, Magnetoelectric Effect in Polar Superconductors, *Phys. Rev. Lett.* **75**, 2004 (1995).
- [39] V. M. Edelstein, Magnetoelectric effect in dirty superconductors with broken mirror symmetry, *Phys. Rev. B* **72**, 172501 (2005).
- [40] A. G. Mal'shukov and C. S. Chu, Spin hall effect in a Josephson contact, *Phys. Rev. B* **78**, 104503 (2008).
- [41] I. V. Bobkova and A. M. Bobkov, Quasiclassical theory of magnetoelectric effects in superconducting heterostructures in the presence of spin-orbit coupling, *Phys. Rev. B* **95**, 184518 (2017).
- [42] Yu. M. Shukrinov, I. R. Rahmonov, and K. Sengupta, Ferromagnetic resonance and magnetic precessions in φ_0 junctions, *Phys. Rev. B* **99**, 224513 (2019).
- [43] C. Guarcello, D. Valenti, G. Augello, and B. Spagnolo, The role of non-Gaussian sources in the transient dynamics of long Josephson junctions, *Acta Phys. Pol. B* **44**, 997 (2013).
- [44] D. Valenti, C. Guarcello, and B. Spagnolo, Switching times in long-overlap Josephson junctions subject to thermal fluctuations and non-Gaussian noise sources, *Phys. Rev. B* **89**, 214510 (2014).
- [45] In the case of weak proximity effect and large exchange field in F , the critical current temperature-dependence is proportional to $I_c(T) \propto \Delta(T) \tanh[\Delta(T)/(k_B T)]$, where $\Delta(T)$ is the superconducting gap, see for example Eq. (2.37) of Ref. [63]. Thus, to find the temperature corresponding to a given noise intensity, we use this relation, with a zero-temperature value $I_c(0) = 100 \mu\text{A}$.
- [46] J. L. García-Palacios and F. J. Lázaro, Langevin-dynamics study of the dynamical properties of small magnetic particles, *Phys. Rev. B* **58**, 14937 (1998).
- [47] J. Z. Sun, Spin angular momentum transfer in current-perpendicular nanomagnetic junctions, *IBM J. Res. Dev.* **50**, 81 (2006).
- [48] D. V. Berkov, in *Handbook of Magnetism and Advanced Magnetic Materials*, edited by H. Kronmüller and S. Parkin (Wiley, New York, 2007), Chap. 2, p. 795823.
- [49] W. T. Coffey and Y. P. Kalmykov, Thermal fluctuations of magnetic nanoparticles: Fifty years after brown, *J. Appl. Phys.* **112**, 121301 (2012).

- [50] M. Nishino and S. Miyashita, Realization of the thermal equilibrium in inhomogeneous magnetic systems by the Landau-Lifshitz-Gilbert equation with stochastic noise, and its dynamical aspects, *Phys. Rev. B* **91**, 134411 (2015).
- [51] J. Leliaert, J. Mulkers, J. De Clercq, A. Coene, M. Dvornik, and B. Van Waeyenberge, Adaptively time stepping the stochastic Landau-Lifshitz-Gilbert equation at nonzero temperature: Implementation and validation in mumax3, *AIP Adv.* **7**, 125010 (2017).
- [52] W. F. Brown, Thermal fluctuations of a single-domain particle, *Phys. Rev.* **130**, 1677 (1963).
- [53] C. Aron, D. G. Barci, L. F. Cugliandolo, Z. G. Arenas, and G. S. Lozano, Magnetization dynamics: Path-integral formalism for the stochastic Landau-Lifshitz-Gilbert equation, *J. Stat. Mech.* **2014**, P09008 (2014).
- [54] R. P. Kaur, D. F. Agterberg, and M. Sigrist, Helical Vortex Phase in the Noncentrosymmetric CePt₃Si, *Phys. Rev. Lett.* **94**, 137002 (2005).
- [55] K. V. Samokhin, Magnetic properties of superconductors with strong spin-orbit coupling, *Phys. Rev. B* **70**, 104521 (2004).
- [56] V. P. Mineev, Magnetoelectric effect and the upper critical field in superconductors without inversion center, *Low Temp. Phys.* **37**, 872 (2011).
- [57] M. Duckheim, D. L. Maslov, and D. Loss, Dynamic spin-hall effect and driven spin helix for linear spin-orbit interactions, *Phys. Rev. B* **80**, 235327 (2009).
- [58] F. Dettwiler, J. Fu, S. Mack, P. J. Weigele, J. C. Egues, D. D. Awschalom, and D. M. Zumbühl, Stretchable Persistent Spin Helices in GaAs Quantum Wells, *Phys. Rev. X* **7**, 031010 (2017).
- [59] J. Clarke and A. I. Braginski, *The SQUID Handbook: Fundamentals and Technology of SQUIDS and SQUID Systems*, The SQUID Handbook No. v. 1 (Wiley, New York, 2004).
- [60] C. Granata and A. Vettoliere, Nano superconducting quantum interference device: A powerful tool for nanoscale investigations, *Phys. Rep.* **614**, 1 (2016).
- [61] D. L. Tilbrook, NanoSQUID sensitivity for isolated dipoles and small spin populations, *Supercond. Sci. Technol.* **22**, 064003 (2009).
- [62] A. Yu. Rusanov, M. Hesselberth, J. Aarts, and A. I. Buzdin, Enhancement of the Superconducting Transition Temperature in Nb/Permalloy Bilayers by Controlling the Domain State of the Ferromagnet, *Phys. Rev. Lett.* **93**, 057002 (2004).
- [63] F. S. Bergeret, A. F. Volkov, and K. B. Efetov, Odd triplet superconductivity and related phenomena in superconductor-ferromagnet structures, *Rev. Mod. Phys.* **77**, 1321 (2005).